HHS Public Access

Author manuscript

Nat Cell Biol. Author manuscript; available in PMC 2014 February 01.

Published in final edited form as:

Nat Cell Biol. 2013 August ; 15(8): 895–904. doi:10.1038/ncb2790.

Role of Telomere Dysfunction in Cardiac Failure in Duchenne Muscular Dystrophy

Foteini Mourkioti[1], **Jackie Kustan**[1], **Peggy Kraft**[1], **John W. Day**[2], **Ming-Ming Zhao**[3], **Maria Kost-Alimova**[4], **Alexei Protopopov**[4], **Ronald A. DePinho**[5], **Daniel Bernstein**[3], **Alan K. Meeker**[6], and **Helen M. Blau**[1]

[1]Baxter Laboratory for Stem Cell Biology, Department of Microbiology and Immunology, Institute for Stem Cell Biology and Regenerative Medicine, Clinical Sciences Research Center, Stanford University School of Medicine, Stanford, CA 94305, USA

[2]Department of Neurology, Stanford School of Medicine, Stanford, CA 94305, USA

[3]Department of Pediatrics (Cardiology), Stanford University, Stanford, CA 94305, USA

[4]Institute for Applied Cancer Science, University of Texas MD Anderson Cancer Center, 1515 Holcombe Blvd, Houston, TX 77030, USA

[5]Department of Cancer Biology, University of Texas MD Anderson Cancer Center, 1515 Holcombe Blvd, Houston, TX 77030, USA

[6]Department of Pathology, Department of Oncology, Johns Hopkins Medical Institution, Baltimore, MD 21231, USA

Abstract

Duchenne Muscular Dystrophy (DMD), the most common inherited muscular dystrophy of childhood, leads to death due to cardiorespiratory failure. Paradoxically, *mdx* mice with the same genetic deficiency of *dystrophin*, exhibit minimal cardiac dysfunction, impeding the development of therapies. We postulated that the difference between *mdx* and DMD might result from differences in telomere lengths in mice and humans. We show here that, like DMD patients, mice that lack dystrophin and have shortened telomeres (*mdx/mTR*^{KO}) develop severe functional cardiac deficits including ventricular dilation, contractile and conductance dysfunction, and accelerated mortality. These cardiac defects are accompanied by telomere erosion, mitochondrial fragmentation, and increased oxidative stress. Treatment with anti-oxidants significantly retards

Corresponding author: Helen M. Blau, Ph.D., Baxter Laboratory for Stem Cell Biology, Stanford University School of Medicine, 269 Campus Drive, CCSR 4215, Stanford, CA 94305, USA, Tel: 650-723-6209, FAX: 650-736-0080, hblau2@stanford.edu.

CONTRIBUTIONS

F.M. designed the studies and performed the experiments, J.K. performed mouse work, histology, immunohistochemistry, mitochondrial quantification analysis and design of cartoons, P.K. maintained the mouse colony and performed histological sections, F.M., A.K.M., M.A. and R.A.D. aided with telomere analyses in mouse samples, F.M. and A.K.M. performed the telomere analysis in human samples, F.M. and D.B. performed the ECG analyses, F.M. and M.Z. performed the osmotic minipump experiments, J.W.D. provided human cardiac samples, F.M. and H.M.B. designed the experiments, discussed and interpreted the results, and wrote the paper with input from A.K.M., R.A.D. and D.B.

COMPETING FINANCIAL INTERESTS

The authors declare no competing financial interests

the onset of cardiac dysfunction and death of *mdx/mTR*^{KO} mice. In corroboration, of four DMD patients analyzed, all had 45% shorter telomeres in their cardiomyocytes relative to age- and sex-matched controls. We propose that the demands of contraction in the absence of dystrophin coupled with increased oxidative stress conspire to accelerate telomere erosion culminating in cardiac failure and death. These findings provide strong support for a link between telomere length and dystrophin deficiency in the etiology of dilated cardiomyopathy in DMD and suggest preventive interventions.

Duchenne muscular dystrophy (DMD) is a lethal X-linked recessive disease that affects 1 in 3,500 live born boys. DMD is characterized by severe progressive muscle wasting due to mutations in dystrophin, which links the inner cytoskeleton with the extracellular matrix and therefore plays a key role in plasma membrane integrity in both skeletal and cardiac muscles [1,2]. Loss of dystrophin destabilizes the membrane, which leads to increased muscle fragility and renders muscle cells highly susceptible to contraction-induced injury [3]. Although DMD is diagnosed based on early skeletal muscle symptoms, progressive cardiorespiratory failure is the primary cause of death, generally in the third decade of life [4–7]. Because the specific mechanisms underlying heart failure in DMD patients are poorly understood, current treatments entail supportive heart failure strategies such as administration of angiotensin-converting enzyme (ACE) inhibitors and β-adrenergic blockers [8,9].

Crucial to our understanding of the molecular mechanisms that underlie the development of DMD and to the design of preventive and therapeutic regimens are animal models that are engineered with tissue-specific mutations that phenocopy the human disease. The most commonly used animal model of DMD is the *mdx* mouse, in which a nonsense mutation in the dystrophin gene eliminates expression of dystrophin [10]. Despite the absence of dystrophin in skeletal and cardiac muscles of *mdx* mice [10], these animals fail to recapitulate the hallmark features of DMD, including severe muscle weakness, progressive cardiomyopathy and shortened life-span [6,7,11,12], severely limiting the utility of the model. A mouse model that more closely resembles the human disease would be invaluable, both for elucidating the pathophysiologic mechanism of cardiac failure in DMD and for the development of more efficacious therapies that target the heart.

A major difference between humans and laboratory mice is the length of their telomeres, specialized DNA-protein complexes comprised of tandem G-rich repeats and located at the ends of eukaryotic chromosomes, which serve to cap and protect chromosome ends [13]. For unknown reasons, telomere lengths differ among species, ranging from ~5–15 kb in humans to >40 kb in mice [14,15]. Telomere shortening occurs during aging and leads to “uncapping”, activating senescence and apoptotic programs which compromise the function of organs with high rates of proliferation and turnover [16]. By deleting the RNA component TERC (mTR) of telomerase, mTR^{KO} mice have been generated that are characterized by a progressive shortening of telomeres, which occurs in the germ line over successive generations (G1–G6). Indeed, ubiquitous shortening of telomeres by successive inbreeding of telomerase deficient mice (*mTR*^{KO}) reveals defects in a range of both proliferative and low-mitotic tissues, similar to aging humans [16].

Given the established link between telomere dysfunction and proliferative defects [16], we previously postulated that deficiency of a single key protein (such as dystrophin) might be unmasked in specific cell types (such as muscle) in mice with moderately reduced telomere reserve (G1 or G2). We tested this hypothesis by crossing *mdx* mice with mice lacking the RNA component of telomerase (*mdx/mTR*^{KO}). As predicted, telomere shortening depleted the proliferative stem cell reservoir which drives regeneration of damaged dystrophic skeletal muscles and the severe progressive muscle weakness typical of DMD was recapitulated [17].

Here we show that *mdx/mTR*^{KO} mice manifest all of the classic signs of dilated cardiomyopathy and heart failure seen in DMD patients. In contrast to skeletal muscle, the heart is a largely quiescent tissue characterized by low cell turnover [18]. It therefore seemed counterintuitive that a similar mechanism could drive the severe cardiomyopathy seen in DMD. Yet, we found that *mdx/mTR*^{KO} mice at early generations (G1 and G2) are characterized by severe contractile and conductance dysfunction, ventricular dilation, and early death.

A test of the clinical relevance of this model revealed that telomere lengths in cardiomyocytes from four DMD patients are 45% shorter than in cardiomyocytes of age and sex-matched human controls. Together, these results highlight that in a setting of mild ubiquitous telomere shortening, the absence of a single contractile protein, dystrophin, elicits tissue-specific defects and significant telomere shortening in non-proliferative heart muscles. This leads to a cycle of DNA damage and telomere shortening, which in turn leads to accelerated organ failure due to mitochondrial dysfunction and oxidative stress. This finding led us to test treatments with anti-oxidants, which as predicted, delayed the progression of dilated cardiomyopathy and the onset of death in *mdx/mTR*^{KO}. Our results provide insights into the cardiorespiratory defects specific to DMD patients and a murine model for testing treatments which will likely impact the quality of life and survival of patients.

RESULTS

We generated dystrophic mice lacking telomerase activity by crossing *mTR*^{Het} mice (lacking one copy of the RNA component of telomerase, known as *mTR* or Terc [19]) with the exon 53 dystrophin mutation known as C57BL6 *mdx*^{4cv} [20] (hereafter designated as *mdx*) as previously described [17]. Rigorous breeding strategies are critical to generate the appropriate controls and consistent phenotypes across generations (Supplementary Figure S1a). Our breeding scheme yields *mdx/mTR*^{KO} mice with a genetic background identical to control *mTR*^{KO} mice, which is critical, as telomere length differs among mouse strains [15]. Since the human disease is X-linked [21], our studies were restricted to male mice. Importantly, the cardiac dystrophic phenotype was compared in mice of all genotypes at the same age and generation, as telomere shortening increases in *mTR*^{KO} mice with successive generations. Double mutant mice lacking dystrophin and telomerase at first and second generation (*mdx/mTR*^{G1} and *mdx/mTR*^{G2} hereafter designated as G1 or G2, respectively) were compared with controls of the same generations: i) C57BL6 wild type mice (WT), ii)

heterozygous mice *mdx/mTR*^{Het} (Het) (lacking dystrophin completely -hence *mdx*- and expressing one allele encoding TERC), and iii) homozygous TERC null mice (*mTR*^{KO}).

Cardiac dilation and premature death in G2 animals

DMD is characterized by a progressive dilated cardiomyopathy with left ventricular wall thinning and increased diameter [22]. Analysis of hearts from young (8- and 20-week-old) *mdx/mTR*^{G2} (G2) mice revealed no obvious abnormalities in cardiac morphology (data not shown), however, by 32 weeks, increased left ventricle enlargement was evident in G2 hearts (Fig. 1a and b) relative to controls. Histologic and morphometric analysis of 32-week-old G2 hearts revealed extensive ventricular fibrosis (Fig. 1b, c) in agreement with reports that extensive fibrosis and scarring, generally localized to the wall of the left ventricle (LV), are the most prevalent cardiac histological features in end-stage DMD patients [22]. Heart-to-body weight and heart-to-tibia length ratio measurements revealed minimal compensatory hypertrophy in G2 animals (Supplementary Fig. S1b), consistent with the human disease. Cardiomyocyte nuclear area was moderately reduced in G2 hearts (Supplementary Fig. S1d and e) and the cardiomyocyte diameter of G2 hearts was smaller than controls (Supplementary Fig. S1d and f). Organ-to-body weight ratios for other organs (lungs, testis, liver, spleen) were unaffected (Supplementary Fig. S1c). These data show that the dilated cardiomyopathy seen in G2 hearts is not due to a systemic effect associated with premature aging and severe functional and anatomic deficits in multiple organs.

Kaplan-Meier survival analysis demonstrated that the life span of *mdx/mTR*^{KO} mice is significantly reduced compared to controls (Fig. 1d). Death first occurs at 30 weeks with a t_{50} of 120 weeks in G1 mice and as early as 19 weeks of age with a t_{50} of 80 weeks of age in G2 mice. In contrast, controls including WT, Het, and *mTR*^{G2}, demonstrated a normal life span (Fig. 1d). Together, these data indicate that dystrophin deficiency in combination with critically shortened telomeres recapitulates the features of dilated cardiomyopathy and reduced lifespan seen in patients with DMD [22].

Cardiac dysfunction in G2 animals

To assess cardiac function, echocardiography was performed. Left ventricular (LV) contractility of G2 mice, measured as percent fractional shortening (%FS), was progressively impaired as a function of age. Echocardiograms for control and double knockout mice showed no significant differences at 12 weeks (Supplementary Fig. S2a) and 20 weeks of age (Supplementary Fig. S2b), but by 32 weeks, G2 mice exhibited a significant reduction in fractional shortening (%FS) relative to controls (32 ± 5 % vs. 55 ± 3 %, respectively) (Fig. S2a, Supplementary Video 1). Two measurements of left ventricular size showed chamber dilation in G2 mice. Left ventricular transverse area in diastole (LVTAd) was moderately increased in G2 mice relative to controls (14 ± 2 mm^2 vs. 8 ± 2 mm^2, respectively). Left ventricular transverse area in systole (LVTAs) was also increased (12 ± 2 mm^2 vs. 4 ± 2 mm^2, respectively) (Fig. 2a and b). Together these data show that cardiac contractile function is impaired and left ventricular chamber size is increased in G2 hearts. Additionally, markers of cardiac failure, including atrial natriuretic peptide (ANP) and brain natriuretic peptide (BNP), were significantly elevated in G2 mice compared to controls at 32 weeks (Fig. 2c), confirming progression to heart failure. Moreover, in response to stress

(Angiotensin II infusion), cardiac dysfunction was induced in younger G2 mice (Supplementary Fig. S3). Notably, although at 32 weeks, G1 mice have normal cardiac function (Fig. 2b), older G1 mice (80 weeks) have significantly reduced cardiac function (FS, LVTAd and LVTAs) relative to controls (Supplementary Fig. S2c). In accordance, *mdx/mTR* mice at G3 (8 weeks) exhibit similar cardiac dysfunction much earlier than *mdx/mTR* mice at G2 (32 weeks) (Supplementary Fig. S2c), indicating that telomere shortening plays an integral role in the cardiac functional defects.

Electrocardiograms (ECGs), a measure of cardiac electrical conduction, revealed delayed conduction in both G1 and G2 mice, evidenced by a wide QRS interval compared to controls (Fig. 2d), indicating a significant ventricular depolarization defect in *mdx/mTR*^{KO} hearts, consistent with findings seen in DMD patients [23]. By contrast, age-matched WT, Het, and *mTR*^{G2} control mice had normal QRS durations (Fig. 2d), providing further evidence that the observed electrical dysfunction results from the combined impact of dystrophin and telomere dysfunction.

Magnetic resonance imaging (MRI) provides dynamic visualization of systolic myocardial wall thickening, and the extent of relaxation and contraction in diastole and systole, respectively [24]. The results of MRI analyses were in accordance with the data obtained by echocardiography and showed that G2 mice exhibit reduced left ventricular systolic function (Fig. 2e). Together, the impaired contractile function, detected by echocardiography and MRI, the prolonged depolarization evident by ECG, the increase in heart failure markers, and early mortality indicate that the hearts of G2 mice become progressively dysfunctional.

Reduction in cardiomyocyte telomere length in G2 mice

To verify that cells within the hearts of G2 mice had shortened telomeres, we utilized a highly sensitive method for determining telomere length in tissue sections, telomere quantitative fluorescence in situ hybridization (Telomere Q-FISH). This method has been used to obtain quantitative telomere length measurements both in murine [25,26] and human cells [27–29]. We optimized fixation methods that enabled Telomere Q-FISH to measure telomere length in combination with immunostaining of a marker of cardiomyocytes (cardiac Troponin T) (Fig. 3a and Supplementary Fig. S4a). A highly significant 50% reduction in telomere length was evident in G2 cardiomyocytes relative to control (WT, Het) and G1 cardiomyocytes (Fig. 3b). By contrast, control *mTR* at generation 2 (*mTR*^{G2}-lacking only TERC) cardiomyocytes exhibited a moderate reduction in telomere lengths, in agreement with studies by others [30, 31], which do not report significant shortening until generations 4 and 5, demonstrating that the dystrophin mutation exacerbates telomere attrition.

To address whether telomere dysfunction in the smooth muscle of cardiac vessels contributes to the cardiac phenotype, we performed telomere Q-FISH in combination with immunostaining of a marker of vascular smooth muscle, α-smooth muscle actin (Supplementary Fig. S4b and c). No significant differences in telomere lengths were evident in vascular smooth muscle cells of the different genotypes (Supplementary Fig. S4b and c). The standard control for Q-FISH was performed on testis (Supplementary Fig. S4d), as cell proliferation is ongoing in this tissue and it is the first to show a reduction in telomere

lengths or weight. In all genotypes (including *mdx/mTR*^{G2} and *mTR*^{G2}), no significant differences were seen in telomere lengths (Supplementary Fig. S4e), tissue morphology [17], or organ weight (Supplementary Fig. S1c), indicating that global telomere shortening is not the basis for the observed phenotype. These data highlight that the enhanced telomere shortening is specific to cardiac (not smooth) muscle cells in the heart, and is not a systemic effect.

Reduction in human cardiomyocyte telomere length in DMD hearts

To test whether our findings in the mouse model were relevant to human DMD, we analyzed postmortem (<24 hours) cardiac tissues from 4 DMD patients (13, 15, 17 and 19 year-old males). Telomere Q-FISH was performed in paraffin sections to assess telomere length in combination with immunostaining for the cardiac marker Troponin T and nuclear DAPI stain (Fig. 4a and Supplementary Fig. S4f). Telomere lengths in human DMD cardiomyocytes were significantly reduced by 45%, ($p<0.005$) compared to cardiomyocytes from three postmortem control hearts (20, 25 and 30 year-old males without cardiac disease) (Fig. 4b). Similar to the *mdx/mTR* mouse model, telomere Q-FISH combined with α-smooth muscle actin immunostaining (Supplementary Fig. S4g and h), demonstrated no significant difference in telomere length in the smooth muscle cells of cardiac vessels. These data validate the *mdx/mTR*^{KO} mouse as a biologically relevant model of human Duchenne Muscular Dystrophy and provide evidence that telomere shortening in DMD patients is specific to cardiomyocytes.

Telomere dysfunction combined with dystrophin mutation induces mitochondrial dysfunction and induces oxidative stress

Although increased cardiomyocyte proliferation or apoptosis did not account for the observed cardiac dysfunction (Supplementary Fig. S5), we observed profound mitochondrial aberrations. Mitochondrial compromise [31–33] and oxidative stress [34–37] have previously been implicated in myocardial dysfunction. Moreover, a strong link between telomere dysfunction and impairment of mitochondrial ultrastructure and organ function, indicative of aging, was shown for liver and heart in mice lacking only telomerase at late generations (e.g. G4) [30]. We therefore investigated the hypothesis that the dilated cardiomyopathy in mice at early generations (e.g. G2) lacking telomerase and dystrophin is associated with mitochondrial dysfunction and oxidative stress. To assess whether telomere shortening in cardiomyocytes induces mitochondrial abnormalities in G2 mice, we performed electron microscopic (EM) analysis. Hearts from G2 animals displayed multifocal abnormalities including a loss of thick as well as thin myofilaments (Fig. 5a), and a moderately increased number of mitochondria (data not shown) combined with decreased mitochondrial size (Fig. 5b). Most notably, the morphology of the mitochondria was highly aberrant, evident by the extensive fragmentation of mitochondria in G2 relative to control mice and lack of well-defined cristae (Fig. 5a and 5b). Our data suggest that mitochondrial abnormalities are accelerated in G2 mice lacking both telomerase and dystrophin, and strongly correlate with the observed cardiac dysfunction leading to early cardiac failure.

To determine if the mitochondrial aberrations evident in the hearts of G2 mice at 32 weeks of age were mediated by the master mitochondrial regulators peroxisome proliferator

activated receptor gamma co-activator 1 alpha (PGC1α) and beta (PGC1β), we assayed their expression by quantitative RT-PCR. As expected, PCG1α and 1β levels were moderately diminished relative to control *mTR*^{KO} mice lacking only telomerase at generation two (~50%), in agreement with a previous report [30]. Notably, however, expression levels of PCG1α and 1β in G2 mice lacking both telomerase and dystrophin (*mdx/mTR*^{KO}) were profoundly reduced (~80%) (Fig. 5c). These data indicate that the cardiac phenotype of mice lacking telomerase is exacerbated by the high metabolic demands of contraction in the absence of dystrophin.

To determine if the mitochondrial compromise and dilated cardiomyopathy seen in G2 mice was accompanied by increased oxidative stress, we stained cardiac tissue sections for 8-hydroxy-deoxyguanosine (8-OHdG), a marker of oxidative damage [38–40]. A significant increase in the number of 8-OHdG-positive nuclei was detected in G2 hearts compared to controls (Fig. 5d and e), indicating that oxidative stress is increased in G2 hearts. In agreement with this finding, expression of superoxide dismutase 1 and 2 (SOD1 and SOD2), genes with anti-oxidant function, were significantly decreased (Fig. 5f), providing additional evidence of augmented oxidative stress in G2 hearts. Notably, mitochondrial function and oxidative stress are exacerbated by telomere dysfunction in combination with dystrophin mutation in G2 mice, leading to lethal cardiomyopathy.

Amelioration of cardiac dystrophic phenotype after anti-oxidant treatment

To determine whether oxidative stress plays a role in the pathogenesis of G2 hearts, we subjected mice to two different anti-oxidants. The first was administrated in the diet (Butylated hydroxyanisole, (BHA) [38] and the second, (Mn(III) tetrakis (4-benzoic acid) porphyrin chloride (MnTBAP) that specifically targets mitochondria [41], was injected intraperitoneally daily (Fig. 6a). G2 mice treated with either anti-oxidant exhibited prolonged survival (Fig. 6b and e) and substantial amelioration of left ventricular function by echocardiography (fractional shortening (FS) (Fig. 6c and f; Supplementary Fig. S6d) relative to untreated G2 mice. MnTBAP was more potent than BHA by all functional measures and exhibited a reduction in fibrotic tissue and heart weight (Supplementary Fig. S6a, b and c). Moreover, transmission electron micrographs of longitudinal cardiac sections revealed improved mitochondrial cristae and morphology in MnTBAP treated hearts compared to saline treated G2 controls (Fig. 6d). Together, these findings demonstrate that administration of anti-oxidants ameliorates both morphological and functional defects and significantly delays the progression of dilated cardiomyopathy in *mdx/mTR*^{KO} mice. These results suggest that the oxidative stress generated in the dystrophic heart is likely to play a causal role in cardiac dysfunction and is a potential early target for treatment in DMD patients.

DISCUSSION

Patients with DMD typically die from cardiorespiratory failure, yet most therapeutic strategies in development currently target the skeletal muscles. Although generally diagnosed based on skeletal myopathic symptoms, the cardiac defect warrants attention and early intervention. 50% of DMD patients 6–10 years of age exhibit abnormal

electrocardiograms (ECG) [23] and by mid- to late-teenage years progressive cardiac dysfunction is common [4–7,23]. Hearts from DMD patients are often characterized by multifocal areas of degenerative changes, characterized by mitochondrial disorganization with loss or discontinuity of cristae, fatty infiltration and loss of myofibers [23,42]. Virtually all DMD patients develop dilated cardiomyopathy and cardiac arrhythmia by the end of their lives [7]. Since DMD patients now survive longer due to increased options for supportive care [7,43], early treatments to prevent or limit the progressive dilated cardiomyopathy, which is now the leading cause of death, are highly desirable. However, the absence of a mouse model of DMD that faithfully mimics the pathophysiology of the human cardiomyopathy has limited our understanding of the underlying mechanisms and ability to test cardiac-specific therapies.

The development of a mouse model that recapitulates lethal human DMD has been hindered for decades, as *mdx* mice (dystrophin deficiency alone) have a surprisingly mild phenotype. A number of more severe dystrophic phenotypes have been created by breeding the *mdx* mouse with utrophin [44], MyoD [45], α7-integrin [46], α-dystrobrevin [47], and a glycan-processing [48] knockout mouse. These other mouse models have been instructive and highly useful in augmenting our knowledge of muscle development and pathophysiology, as well as serving as useful test systems for therapeutic interventions. However, these models [44–47], disrupt proteins essential for skeletal and/or cardiac muscle function that are not mutated or lost in DMD patients. An advantage of the *mdx/mTR*^{KO} mouse model described here is that lack of dystrophin is coupled with somewhat shortened telomeres, as seen in humans with DMD. Mouse models that mimic other human genetic degenerative diseases [49,50] associated with DNA repair (ataxia-telangiectasia) were first generated when bred with mice with shortened telomeres. Here we show that the *mdx* mouse manifests all of the major hallmarks of human DMD once bred with mice that lack telomerase (*mTR*) yielding *mdx* mice with shortened telomere (*mdx/mTR*^{KO}).

This report provides the first evidence for a cardiac phenotype in a mouse model of DMD and a conceptual basis for the disease mechanism. We previously reported that combined dystrophin and telomerase deficiency leads to a skeletal myopathy similar to that observed in human DMD, due to a chronic cycle of myofiber damage and repair that ultimately led to a loss of the stem cell reservoir due to the shortened telomeres [17,51]. Here we show that this model manifests essentially all features of cardiomyopathy described in DMD patients [7,22,52], including cardiac dilation, prolonged ventricular depolarization and decreased systolic function. We report ultrastructural changes in mitochondria, mitochondrial dysfunction including decreased levels of peroxisome proliferator-activated receptor gamma, co-activator 1 alpha and beta (PCG1α and 1β) and markers of oxidative compromise (decreased SOD and increased 8-OHdG) in *mdx/mTR*^{KO} mice. Although these changes are typically associated with cardiomyopathy and heart failure of diverse etiologies [53,54] and shortened telomeres have also been detected in the hearts of patients with heart failure [55], this is the first report showing that these features can result from progressive telomere erosion, specifically in cardiomyocytes due to the genetic absence of a single crucial cardiac-specific gene product. Notably, telomere shortening was not detected in other muscle cells of the heart, such as those of the vasculature, providing further support

for the specificity of telomere dysfunction in cardiomyocytes in the etiology of the disease. These defects culminate in dilated cardiomyopathy and heart failure with an onset of death by 19 and 32 weeks of age, in G1 and G2, respectively. The importance of telomere shortening in the etiology of dilated cardiomyopathy is underscored by our finding of shortened telomeres (45%) in the cardiomyocytes in four DMD patients (which lack dystrophin) compared to controls (which express dystrophin).

Our data suggest that oxidative stress is a critical step in the pathogenesis of cardiac failure in patients with muscular dystrophy since antioxidants can ameliorate the major features of dilated cardiomyopathy and improve life-span in our model. Moreover, although respiratory and skeletal muscle failure likely contribute to the observed cardiac phenotype, our findings highlight an intrinsic cardiac defect. Based on our results, we postulate that the *mdx/mTR*^{G2} mouse model sets in motion a cycle whereby (1) stress is initiated by absence of dystrophin during continuous cycles of cardiac contraction in conjunction with short telomeres (already shortened in humans) which (2) induces mitochondrial compromise and increased oxidative stress which (3) then leads to further telomere erosion and progression to lethal dilated cardiomyopathy. We postulate that as in DMD, shortened telomeres may well exacerbate other heritable tissue-specific protein deficits, as the long telomeres typical of mice may 'mask' their manifestation. The findings reported here increase our understanding of DMD and will facilitate the development and testing of therapies targeted to treat or prevent the onset of heart failure and death.

Online Methods

Mice

All protocols were approved by the Stanford University Administrative Panel on Laboratory Animal Care. C57BL6 *mdx*^{4cv} mice [20] and C57BL6 *mTR*^{Het} mice [19] were used to generate the double mutant animals as described in Supplementary Figure 1a. Genotyping was performed by PCR as described previously [17]. Since the human disease is X-linked [21], our studies were restricted to male mice. The exact number of animals for each data set and all relevant details regarding the sample size are reported with each experiment.

ECG analysis

ECGs were recorded to assess intra-LV conduction using Chart for Windows v4.1 (AD Instruments, Colorado Springs, CO) as described previously [57]. ECGs were recorded from needle electrodes inserted subcutaneously in the chest and secured with tape. If the ECG was abnormal, other positions were used to validate and/or further characterize the ECG abnormality. The signal was acquired for 1 minute and in 3 different electrode chest positions/mouse. During offline analysis, we examined the 1-minute recording for unusually shaped QRS and for time-varying phenomenon (e.g. irregularities in interval durations). Ectopic or abnormal beats were noted. A representative 10–15 s segment of the recording was averaged to obtain the signal averaged ECG.

Echocardiographic analysis

Animals were anesthetized with isoflurane (1.5% in O_2) and the left hemithorax was shaved. The mice were placed on a temperature-controlled pad and heart rate was continuously monitored (400–550bpm). Ultrasound transmission gel (Parker Laboratories Inc.) was used and the heart was imaged in the parasternal short-axis view. Two-dimensional B-mode and M-Mode images were obtained at the papillary muscle level using the Vevo 770 Ultrasound system (VisualSonics) and left ventricular transverse area in systole (LVTAs), left ventricular transverse area in diastole (LVTAd), and fractional shortening (FS) were calculated using the using Vevo 770 V2.2.3 software (VisualSonics). All analyses were performed with the investigators blinded to genotype.

MRI analysis

Magnetic resonance imaging (MRI) was performed at the Stanford Clark Center Small Animal Imaging Facility in a self-shielded Varian/General Electric “microSigna 7.0” 7T, 310 mm (horizontal) bore scanner (Varian Inc., Palo Alto, CA, USA/GE Healthcare, Waukesha, WI, USA), including Copley gradient drivers, EXCITE2 electronics; the supporting LX11 platform; and a custom-built quadrature birdcage radio frequency (RF) coil. Animals were anesthetized with 2% isoflurane in humidified medical grade oxygen. Physiological respiration and temperature feedback was carefully monitored and cardiac acquisitions were gated to the cardiac cycle. The animal was placed on an animal bed while kept under anesthesia. During the scan, the heart rate, respiration and ECG signals were monitored closely. Transverse cardiac images were acquired with a fast gradient echo (fgre) sequence, a flip angle of 20 degrees, repetition time of 200 ms, echo time of 0.9 ms, slice thickness of 1 mm, 3 cm FOV with a 256×256 matrix, and a number of excitations (averages) of 2. Image analysis performed using the open source software Osirix (http://www.osirixviewer.com).

Electron microscopy

Samples were fixed in Karnovsky’s fixative: 2% Glutaraldehyde (EMS) and 4% paraformaldehyde (EMS) in 0.1M Sodium Cacodylate (EMS) pH 7.4 for 1 hr at RT then cut, post-fixed in 1% Osmium tetroxide (EMS) for 1 hr at RT, washed 3 times with ultra-filtered water, then en bloc stained for 2 hrs at RT or moved to 4°C overnight. Samples were then dehydrated in a series of ethanol, followed by Acetonitrile for 15 min. Samples are infiltrated with EMbed-812 resin (EMS) mixed 1:1 with Acetonitrile for 2 hrs followed by 2 parts EMbed-812 to 1 part Acetonitrile for 2 hours. The samples were then placed into EMbed-812 for 2 hours then placed into molds and resin filled gelatin capsules w/labels were orientated properly and placed into 65°C oven overnight. Sections were taken between 75 and 90nm on a Leica Ultracut S (Leica, Wetzlar, Germany) and grids were contrast stained for 15 minutes in 1:1 saturated UrAcetate (~7.7%) to 100% Ethanol followed by staining in 0.2% Lead Citrate for 3 minutes. Photos were taken using a Gatan Orius digital camera.

Chronic angiotensin administration

Osmotic minipumps (Alzet 2004) filled either with Angiotensin II (0.9 μg/h, Sigma A9525) or 0.9% saline were implanted subcutaneously into each mouse, as described previously [58].

Cardiac morphology and morphometric analysis

Hearts were excised at the indicated ages and fixed over-night at 4% paraformaldehyde. Following progressive tissue dehydration with ethanol and xylene, the heart samples were embedded in paraffin. 7 μm thick cross-sections were subjected to trichrome staining (Sigma-Aldrich) for nuclei, cytoplasm and collagen visualization. Images from randomly chosen fields distributed across the cardiac section were collected using a Zeiss stage microscope (AxionVision) and morphometric analysis for collagen tissue deposition was performed with MetaMorph software (version 6.2r5; Universal Imaging Corporation).

Quantitative RT-PCR (Q-RT-PCR)-based gene expression analysis

Total RNA was isolated from hearts using TRIzol (Invitrogen). RNA was treated with DNaseI enzyme (Promega) for 1h at 37°C and then subjected to column purification (Qiagen). The RNA concentration was determined with a spectrophotometer. After RNA quality verification, 1 μg were used to prepare cDNA (Ready-To-Go, T-Primed First-Strand Kit, Amersham Bioscience 27-9263-01). Inventoried TaqMan FAM probes (Applied Biosystems) were used for the relative quantification of the mRNA levels of ANP (Mm01255747_g1), BNP (Mm00435304_g1), SOD1 (Mm01344232_g1) and SOD2 (Mm00449726_m1), PGC1α (Mm00447184_g1) and 1β (Mm01258517_g1) genes. Taqman VIC Glyceraldehyde 3-phosphate dehydrogenase (GAPDH) probes (4552339E) were used for normalization. Data analysis was performed using the ΔΔC(T) method.

Immunofluorescence microscopy

Slides were deparaffinized in xylene and rehydrated in serial ethanol concentrations. Antigen masking was performed in citrate buffer (10mmol/L sodium citrate, pH 6.0) for 30min in a pressure cooker. Slides were blocked with 5% normal goat serum (DAKO) for 1h at room temperature (RT). Incubation with primary antibody against 8-hydroxy-2′-deoxyguanosine (8-OHdG) (1:20, JaICA), activated caspase-3 (1:50, Abcam ab13847), smooth muscle α-actin (1:200, Abcam ab32575), α-actinin (1:200, Sigma A7811), phospho-Hist3 (1:50, Cell Signaling 9706) and Ki67 (1:100, Dako Clone TEC-3.) was done overnight (O/N) at 4°C. After washing in PBS, the slides were incubated with the appropriate biotinylated-secondary antibody for 60min at RT (for 8-OHdG staining) or with the appropriate Alexa 488 or Alexa 596 secondary antibodies (1:500, Invitrogen) for 1.5 hours in the dark at room temperature. The nuclei were counterstained with DAPI. The slides were again washed in PBS and incubated for 30min with VECTASTAIN ABC-AP reagent (Vector Laboratories). Next, the Vector Blue Alkaline Phosphatase substrate kit was used (Vector Laboratories) in order to visualize the 8-OHdG staining (blue color). Then, slides were dehydrated through serial ethanol concentrations and a xylene-free clearing reagent (National Diagnostics) and mounted permanently. Quantification of 8-OHdG positive nuclei was performed in a blind fashion after acquisition of at least 5 images from the left ventricle of each sample (n=3) at 40x magnification. Background was reduced using brightness and

contrast adjustments, and color balance was performed to enhance colors. All the modifications were applied to the whole image using Adobe Photoshop CS3.

TUNEL assay

Deparaffinized cardiac sections were permeabilized by proteinase K treatment for 30min and re-fixed in 4% paraformaldehyde. After an equilibration step, the 3′-OH end of DNA breaks was labeled with fluorescein-12-dUTP using recombinant Terminal Deoxynucleotidyl Transferase (rTdT) enzyme (Promega G3250) by incubating the slides at 37°C for 1hour. The reaction was terminated in 2X SSC solution and the slides were washed in PBS and mounted with DAPI (Vectashield).

Human cardiac tissue

Control hearts were isolated <24 hours postmortem from deidentified male patients aged 20, 25 and 30 years who succumbed to non-cardiac disease (metastatic sarcoma, sickle-cell anemia, and chronic pancreatitis). The DMD hearts were isolated <24 hours postmortem from de-identified 13 and 15-year old (Harvard), 17-year old (Johns Hopkins) and 19-year old (University of Wisconsin) patients. All samples went through the routine neutral-buffered formalin fixation followed by paraffin embedding. 4μM sections from the paraffin blocks were placed on ChemMate™ slides (Fisher Scientific) for the Telomere Q-FISH analysis. All protocols using human samples were reviewed and approved by the Stanford Institutional Review Board.

Telomere Q-FISH

Telomere Q-FISH. 4μM thick sections of embedded paraffin hearts were cut and preheated to 65°C for 10 minutes and passed through xylene to remove paraffin. Slides were hydrated through a graded ethanol series, deionized water and then immersed for 60 sec in dH_2O with 1% Tween-20 detergent, followed by immersion in citrate buffer pH 6.0 in a steamer for 35 min. After cooling, slides were immersed in dH2O, 70% ethanol, 95% ethanol, and then let to dry at RT. 35μl diluted PNA probe hybridization solution (0.3 μg/ml Cy3-labeled Telomere PNA; 0.3 μg/mL FITC-labeled Centromere PNA (both probes custom synthesized by Bio-Synthesis, Inc.) were placed onto the specimen. After denaturation (84°C, 5 min), slides were left o/n to hybridize (dark). Next, slides were washed twice with PNA Wash Solution (Formamide, 1M Tris pH 7.5 and dH2O), PBST and were blocked for 1h with blocking solution (Invitrogen). Afterwards, slides were incubated for 1h at RT with primary antibodies: anti-mouse α-cardiac Troponin T (1:100, Abcam) or anti-rabbit α-smooth muscle (1:100, Abcam), washed with PBST, incubated with secondary antibodies: anti-mouse IgG fraction Alexa Fluor 488 (Molecular Probes) or anti-rabbit IgG fraction Alexa Fluor 488 (Molecular Probes) for 30 min, counter stained with 1 μg/ml DAPI solution in dH_2O, washed in dH_2O, air dried and mounted (ProlongTM, Molecular Probes). To avoid differences in day-to-day staining efficiency variation, Q-FISH and immuno-Q-FISH staining as well as the image capture were performed on the same day. To control for differences in ploidy and probe accessibility, FITC-labeled PNA probes were used that recognize centromeric major satellite repeats, as described previously [28,29]. DAPI staining was used to define nuclear area and for quantification of DNA content and Cy3 staining was used to quantify telomere fluorescence. Telomere fluorescence signals for individual cells of

interest were identified by overlay of the DAPI image. Omega Optical XF38 filter set (Omega Optical Incorporated) for Cy3 visualization was used as described in [29]. The range of focal planes was examined on the Z-axis to determine that cardiomyocyte nuclei were within the striated muscle. Images were acquired at 40x. The investigators were blinded to genotype of the sections analyzed. Data were analyzed using the "Telometer: Software for Telomere Counting" as described previously at http://demarzolab.pathology.jhmi.edu/telometer/. The algorithm developed at Johns Hopkins performs subtraction of background noise of the entire image, distinction of the individual telomere spots, removal of halos and separation of conjoined telomeres. The program generated statistics on the entire region of the nucleus, as well as each individual telomere in the nucleus. Statistics returned include the intensity sum of all Cy3 telomere pixels for a given nucleus (proportional to telomere length) and the intensity sum of all DAPI pixels for the nucleus (proportional to total nuclear DNA content). By taking the ratio of the telomere intensity sum to the corresponding DAPI intensity sum one is able to compensate for ploidy differences as well as the variable fractions of nuclei present in the cutting plane of the tissue section.

Antioxidant Treatments

The commonly used 2018 Global diet (Mucedola srl) was used as normal diet, whereas the antioxidant diet was the same 2018 Global diet only supplemented with 0.7% of the antioxidant compound butylated hydroxyanisole (BHA) (Sigma). Both normal and antioxidant food were weighed every day to ensure similar food intake in all the experimental groups of the animals. In a second experiment using the alternative antioxidant Mn(III) tetrakis (4-benzoic acid) porphyrin chloride (MnTBAP), mice were treated every other day until 42 weeks of age with 10 mg/kg) MnTBAP intraperitoneally or saline vehicle. Antioxidant treatments provided at 8 weeks of age and onwards. Animals were kept in single cages to correlate food reduction in the cage with caloric intake for each mouse. Water was provided daily in graduated bottles to monitor liquid reduction. Detailed monitoring of cardiac function by echocardiography was performed before and monthly during the anti-oxidant treatments. The experiment was terminated between 40–42 weeks of age and the hearts were examined at the histological and molecular level. For each treatment, at least 10 animals were tested per genotype and condition.

Statistical Analysis

Values were expressed as mean ± SEM and differences with P value < 0.05 were considered significant (* P < 0.05, ** P < 0.01, *** P < 0.001). Comparisons between two groups were performed using the Student's *t*-test (tail 2, type 2 or 3). Repeated measures experiments were analyzed by ANOVA followed by Bonferonni's post-hoc corrections. All statistical analyses were performed using Excel or GraphPad Prism software. Source data are shown in Supplementary Table S1.

Supplementary Material

Refer to Web version on PubMed Central for supplementary material.

Acknowledgments

We thank Dr. Euan Ashley (Director, Stanford Center for Inherited Cardiovascular Disease), Dr. John Cooke (Associate Director of Cardiovascular Institute, Stanford), Dr. Michael V. McConnell (Cardiovascular Medicine, Stanford), Dr. Andrew Connolly (Pathology, Stanford), Dr. Steve Artandi (Medicine-Hematology, Stanford), and Dr. Jason Pomerantz (Center of Regeneration Medicine and Stem Cell Research, UCSF) for insightful discussions and critical comments. We greatly appreciate the input and thoughtful discussions from all Blau lab members and would like to especially thank Dr. Srihari Sampath for critical comments on the manuscript and Dr. Andrew Tri Van Ho for help with the final formatting of the supplementary videos. We are grateful to Dr. Donald Regula (Department of Pathology, Stanford) for providing the control cardiac samples, Dr. Marc Halushka (Department of Pathology, Johns Hopkins), Dr. Alan H. Beggs (Harvard University) and Dr. Hart Lidov (Department of Pathology, Boston Children's Hospital) for providing us with DMD cardiac samples. Moreover, we are grateful to Muscular Dystrophy Center Core Laboratories at University of Minnesota, the Department of Pathology at Boston Children's Hospital, the DMD patients and their families who contribute to the tissue repository. We thank Eric Neri (Data Manager, Stanford) for computational algorithms for analysis of telomere lengths, Andrew Olson at the NMS ("Stanford Neuroscience Microscopy Service, supported by NIH NS069375"), Kassie Koleckar (Blau lab), and Pauline Chu (Comparative Medicine, Stanford), Laura Jean Pisani (MIPS MRI Physicist, Stanford Small Imaging Facility), John Perrino (Electron Microscopy Facility, Stanford) as well as Reese Zasio and Edward Florendo (Stanford Mouse Facility) for excellent technical assistance. This work was supported by grants from the American Heart Association Scientist Development Grant 10SDG3510024 (F.M.), NIH/NIAMS P30 AR057220 (J.W.D), R01CA84628 (R.A.D.), R.A.D., A.M. and A.P. were supported by the Robert A. and Renee E. Belfer Foundation, NIH Grant HL061535 (D.B.), P50 CA058236 (W. Nelson) NIH SPORE in Prostate Cancer (A.K.M.), and NIH grants HL096113, HL100397, AG020961, and AG009521, MDA grant 4320 and the Baxter Foundation (H.M.B.).

References

1. Liew CC, Dzau VJ. Molecular genetics and genomics of heart failure. Nat Rev Genet. 2004; 5:811–825. [PubMed: 15520791]
2. Hoffman EP, Brown RH Jr, Kunkel LM. Dystrophin: the protein product of the Duchenne muscular dystrophy locus. Cell. 1987; 51:919–928. [PubMed: 3319190]
3. Petrof BJ, Shrager JB, Stedman HH, Kelly AM, Sweeney HL. Dystrophin protects the sarcolemma from stresses developed during muscle contraction. Proc Natl Acad Sci U S A. 1993; 90:3710–3714. [PubMed: 8475120]
4. Bushby K, Muntoni F, Bourke JP. 107th ENMC international workshop: the management of cardiac involvement in muscular dystrophy and myotonic dystrophy. 7th–9th June 2002, Naarden, the Netherlands. Neuromuscul Disord. 2003; 13:166–172. [PubMed: 12565916]
5. Baxter P. Treatment of the heart in Duchenne muscular dystrophy. Dev Med Child Neurol. 2006; 48:163. [PubMed: 16483388]
6. Duan D. Challenges and opportunities in dystrophin-deficient cardiomyopathy gene therapy. Human molecular genetics. 2006; 15(Spec No 2):R253–261. [PubMed: 16987891]
7. McNally EM. New approaches in the therapy of cardiomyopathy in muscular dystrophy. Annu Rev Med. 2007; 58:75–88. [PubMed: 17217326]
8. Cohn JN. Heart failure: future treatment approaches. Am J Hypertens. 2000; 13:74S–78S. [PubMed: 10830793]
9. Cohn RD, et al. Angiotensin II type 1 receptor blockade attenuates TGF-beta-induced failure of muscle regeneration in multiple myopathic states. Nat Med. 2007; 13:204–210. [PubMed: 17237794]
10. Bulfield G, Siller WG, Wight PA, Moore KJ. X chromosome-linked muscular dystrophy (*mdx*) in the mouse. Proc Natl Acad Sci U S A. 1984; 81:1189–1192. [PubMed: 6583703]
11. Bridges LR. The association of cardiac muscle necrosis and inflammation with the degenerative and persistent myopathy of *MDX* mice. J Neurol Sci. 1986; 72:147–157. [PubMed: 3711930]
12. Torres LF, Duchen LW. The mutant *mdx*: inherited myopathy in the mouse. Morphological studies of nerves, muscles and end-plates. Brain. 1987; 110 (Pt 2):269–299. [PubMed: 3567525]
13. Greider CW, Blackburn EH. The telomere terminal transferase of Tetrahymena is a ribonucleoprotein enzyme with two kinds of primer specificity. Cell. 1987; 51:887–898. [PubMed: 3319189]

14. Kipling D, Cooke HJ. Hypervariable ultra-long telomeres in mice. Nature. 1990; 347:400–402. [PubMed: 2170845]
15. Hemann MT, Greider CW. Wild-derived inbred mouse strains have short telomeres. Nucleic Acids Res. 2000; 28:4474–4478. [PubMed: 11071935]
16. Lee HW, et al. Essential role of mouse telomerase in highly proliferative organs. Nature. 1998; 392:569–574. [PubMed: 9560153]
17. Sacco A, et al. Short telomeres and stem cell exhaustion model Duchenne muscular dystrophy in *mdx/mTR* mice. Cell. 2010; 143:1059–1071. [PubMed: 21145579]
18. Bergmann O, et al. Evidence for cardiomyocyte renewal in humans. Science. 2009; 324:98–102. [PubMed: 19342590]
19. Blasco MA, et al. Telomere shortening and tumor formation by mouse cells lacking telomerase RNA. Cell. 1997; 91:25–34. [PubMed: 9335332]
20. Im WB, et al. Differential expression of dystrophin isoforms in strains of *mdx* mice with different mutations. Human molecular genetics. 1996; 5:1149–1153. [PubMed: 8842734]
21. Emery AE. Population frequencies of inherited neuromuscular diseases--a world survey. Neuromuscul Disord. 1991; 1:19–29. [PubMed: 1822774]
22. Finsterer J, Stollberger C. The heart in human dystrophinopathies. Cardiology. 2003; 99:1–19. [PubMed: 12589117]
23. Sanyal SK, Johnson WW. Cardiac conduction abnormalities in children with Duchenne's progressive muscular dystrophy: electrocardiographic features and morphologic correlates. Circulation. 1982; 66:853–863. [PubMed: 7116601]
24. Schneider JE, et al. Fast, high-resolution in vivo cine magnetic resonance imaging in normal and failing mouse hearts on a vertical 11.7 T system. J Magn Reson Imaging. 2003; 18:691–701. [PubMed: 14635154]
25. Flores I, et al. The longest telomeres: a general signature of adult stem cell compartments. Genes Dev. 2008; 22:654–667. [PubMed: 18283121]
26. Gonzalez-Suarez E, Samper E, Flores JM, Blasco MA. Telomerase-deficient mice with short telomeres are resistant to skin tumorigenesis. Nat Genet. 2000; 26:114–117. [PubMed: 10973262]
27. Meeker AK, De Marzo AM. Recent advances in telomere biology: implications for human cancer. Curr Opin Oncol. 2004; 16:32–38. [PubMed: 14685090]
28. Meeker AK, et al. Telomere length assessment in human archival tissues: combined telomere fluorescence in situ hybridization and immunostaining. Am J Pathol. 2002; 160:1259–1268. [PubMed: 11943711]
29. Meeker AK, et al. Telomere shortening occurs in subsets of normal breast epithelium as well as in situ and invasive carcinoma. Am J Pathol. 2004; 164:925–935. [PubMed: 14982846]
30. Sahin E, et al. Telomere dysfunction induces metabolic and mitochondrial compromise. Nature. 2011; 470:359–365. [PubMed: 21307849]
31. Brown DA, O'Rourke B. Cardiac mitochondria and arrhythmias. Cardiovasc Res. 2010; 88:241–249. [PubMed: 20621924]
32. Iglewski M, Hill JA, Lavandero S, Rothermel BA. Mitochondrial fission and autophagy in the normal and diseased heart. Curr Hypertens Rep. 2010; 12:418–425. [PubMed: 20865352]
33. Murdoch CE, Zhang M, Cave AC, Shah AM. NADPH oxidase-dependent redox signalling in cardiac hypertrophy, remodelling and failure. Cardiovasc Res. 2006; 71:208–215. [PubMed: 16631149]
34. Takimoto E, et al. Oxidant stress from nitric oxide synthase-3 uncoupling stimulates cardiac pathologic remodeling from chronic pressure load. J Clin Invest. 2005; 115:1221–1231. [PubMed: 15841206]
35. van Empel VP, et al. Downregulation of apoptosis-inducing factor in harlequin mutant mice sensitizes the myocardium to oxidative stress-related cell death and pressure overload-induced decompensation. Circ Res. 2005; 96:e92–e101. [PubMed: 15933268]
36. Sawyer DB. Oxidative stress in heart failure: what are we missing? Am J Med Sci. 2011; 342:120–124. [PubMed: 21747279]

37. Rasmussen HH, Hamilton EJ, Liu CC, Figtree GA. Reversible oxidative modification: implications for cardiovascular physiology and pathophysiology. Trends Cardiovasc Med. 2010; 20:85–90. [PubMed: 21130951]
38. Kratsios P, et al. Antioxidant amelioration of dilated cardiomyopathy caused by conditional deletion of NEMO/IKKgamma in cardiomyocytes. Circ Res. 2010; 106:133–144. [PubMed: 19850942]
39. Shigenaga MK, Gimeno CJ, Ames BN. Urinary 8-hydroxy-2′-deoxyguanosine as a biological marker of in vivo oxidative DNA damage. Proc Natl Acad Sci U S A. 1989; 86:9697–9701. [PubMed: 2602371]
40. Shirendeb U, et al. Abnormal mitochondrial dynamics, mitochondrial loss and mutant huntingtin oligomers in Huntington's disease: implications for selective neuronal damage. Human molecular genetics. 2011; 20:1438–1455. [PubMed: 21257639]
41. Li Y, et al. Cytosolic, but not mitochondrial, oxidative stress is a likely contributor to cardiac hypertrophy resulting from cardiac specific GLUT4 deletion in mice. FEBS J. 2011
42. Sanyal SK, Johnson WW, Thapar MK, Pitner SE. An ultrastructural basis for electrocardiographic alterations associated with Duchenne's progressive muscular dystrophy. Circulation. 1978; 57:1122–1129. [PubMed: 639232]
43. Finder JD, et al. Respiratory care of the patient with Duchenne muscular dystrophy: ATS consensus statement. Am J Respir Crit Care Med. 2004; 170:456–465. [PubMed: 15302625]
44. Deconinck AE, et al. Utrophin-dystrophin-deficient mice as a model for Duchenne muscular dystrophy. Cell. 1997; 90:717–727. [PubMed: 9288751]
45. Megeney LA, et al. Severe cardiomyopathy in mice lacking dystrophin and MyoD. Proc Natl Acad Sci U S A. 1999; 96:220–225. [PubMed: 9874799]
46. Rooney JE, et al. Severe muscular dystrophy in mice that lack dystrophin and alpha7 integrin. J Cell Sci. 2006; 119:2185–2195. [PubMed: 16684813]
47. Grady RM, et al. Role for alpha-dystrobrevin in the pathogenesis of dystrophin-dependent muscular dystrophies. Nat Cell Biol. 1999; 1:215–220. [PubMed: 10559919]
48. Chandrasekharan K, et al. A human-specific deletion in mouse Cmah increases disease severity in the *mdx* model of Duchenne muscular dystrophy. Sci Transl Med. 2010; 2:42ra54.
49. Qi L, et al. Short telomeres and ataxia-telangiectasia mutated deficiency cooperatively increase telomere dysfunction and suppress tumorigenesis. Cancer Res. 2003; 63:8188–8196. [PubMed: 14678974]
50. Wong KK, et al. Telomere dysfunction and Atm deficiency compromises organ homeostasis and accelerates ageing. Nature. 2003; 421:643–648. [PubMed: 12540856]
51. Chamberlain JS. Duchenne muscular dystrophy models show their age. Cell. 2010; 143:1040–1042. [PubMed: 21183068]
52. Frankel KA, Rosser RJ. The pathology of the heart in progressive muscular dystrophy: epimyocardial fibrosis. Hum Pathol. 1976; 7:375–386. [PubMed: 939536]
53. Esposito LA, Melov S, Panov A, Cottrell BA, Wallace DC. Mitochondrial disease in mouse results in increased oxidative stress. Proc Natl Acad Sci U S A. 1999; 96:4820–4825. [PubMed: 10220377]
54. Narula N, et al. Adenine nucleotide translocase 1 deficiency results in dilated cardiomyopathy with defects in myocardial mechanics, histopathological alterations, and activation of apoptosis. JACC Cardiovasc Imaging. 2011; 4:1–10. [PubMed: 21232697]
55. Brouilette S, Singh RK, Thompson JR, Goodall AH, Samani NJ. White cell telomere length and risk of premature myocardial infarction. Arterioscler Thromb Vasc Biol. 2003; 23:842–846. [PubMed: 12649083]
56. Yin FCP, Spurgeon HA, Rakusan K, Myron L, Weisfeldt, Lakatta EG. Use of tibial length to quantify cardiac hypertrophy: application in the aging rat. Am J Physiol Heart Circ Physiol. 1982; 243:H941–H947.
57. Urashima T, et al. Molecular and physiological characterization of RV remodeling in a murine model of pulmonary stenosis. Am J Physiol Heart Circ Physiol. 2008; 295:H1351–H1368. [PubMed: 18586894]

58. McCalmon SA, et al. Modulation of angiotensin II-mediated cardiac remodeling by the MEF2A target gene Xirp2. Circ Res. 2010; 106:952–960. [PubMed: 20093629]

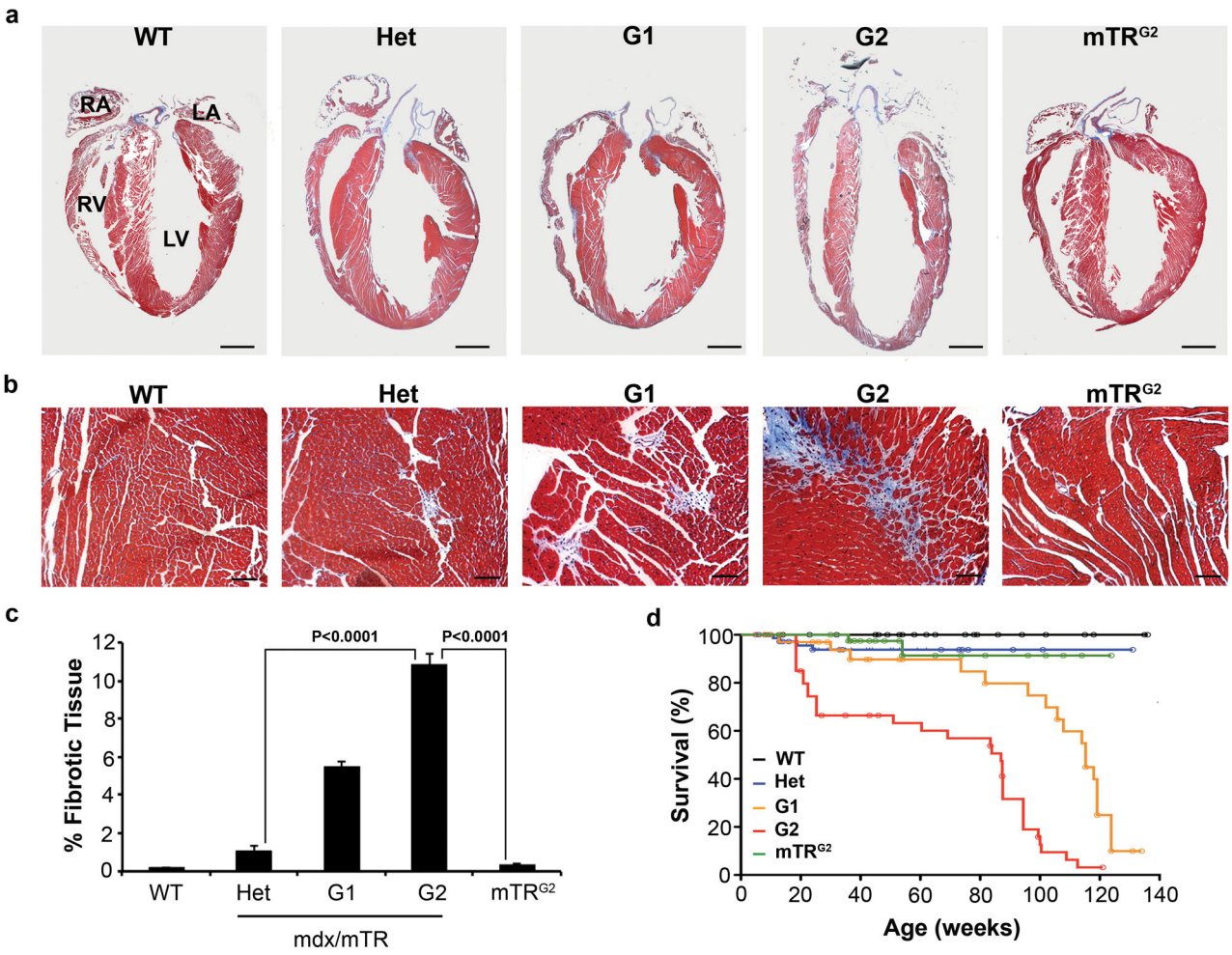

Figure 1. Cardiac dilation, fibrosis and premature death in G2 mice

(a) Trichrome staining in longitudinal paraffin sections of 32-week-old hearts. G2 hearts develop dilated cardiomyopathy accompanied by enlarged ventricular cavity and thinning of the ventricular wall (LV Left Ventricle, RV Right Ventricle, LA Right Atrium, RA Right Atrium). Scale bar 15 μm. **(b)** Increased collagen deposition (blue) in the left ventricle of G2 hearts compared to controls. Scale bar 600 μm. **(c)** Quantification of collagen deposition. Data are represented as mean ± SEM (n=3–4), Two-tailed, unpaired Student's *t*-test, P values are indicated in the graph. **(d)** Kaplan-Meier survival curve shows G2 mice have significantly reduced life span compared to controls. WT (n=72), HET (n=86), G1 (n=45), G2 (n=53) and *mTR*^{G2} (n=45). Source data are shown in Supplementary Table S1.

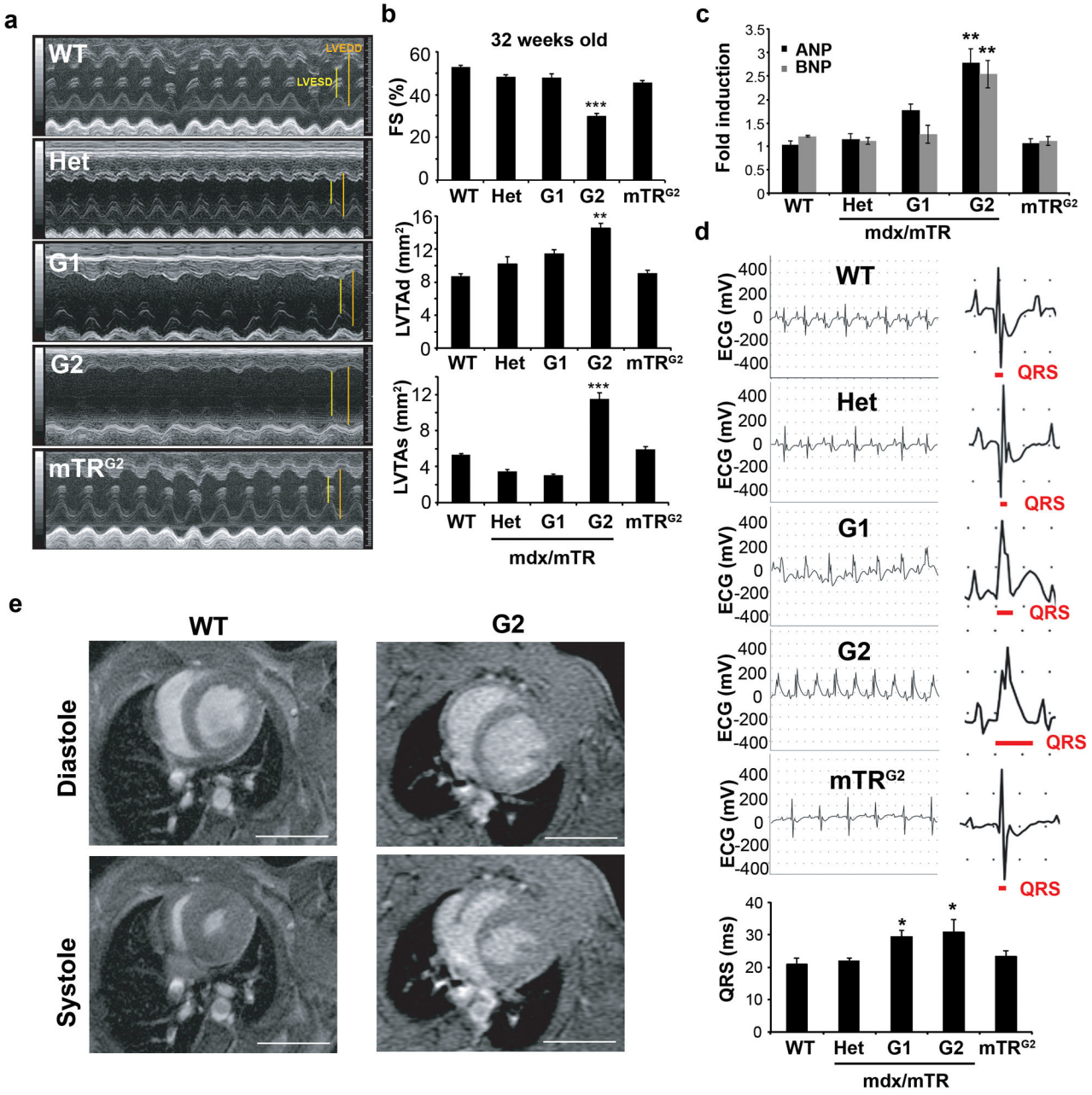

Figure 2. Severe cardiac dysfunction and heart failure in G2 mice

(a) Representative images of 32-week-old hearts showing left ventricular dilation and compromised contractility (LVEDD; Left Ventricular End Diastolic Diameter, LVESD; Left Ventricular End Systolic Diameter). **(b)** Echocardiograph measurements show reduction in fractional shortening (FS), increase in left ventricular transverse area in diastole (LVTAd) and increase in left ventricular transverse area in systole (LVTAs) in 32-week-old G2 hearts compared to control hearts. Data are represented as mean ± SEM (n=5–8), Two-tailed, unpaired Student's *t*-test, ** indicates P <0.01 and *** P<0.001. **(c)** Increased cardiac failure markers ANP and BNP by Q-RT-PCR analysis confirmed heart failure in G2 mice. Data are represented as mean ± SEM (n=3); Two-tailed, unpaired Student's *t*-test, **

indicates P <0.01. **(d)** Representative electrocardiograms (ECG) of 32-week-old hearts show impairment in ventricular depolarization of G1 and G2 hearts manifested by a prolonged QRS interval. Lower graph shows quantification of QRS values. Data are represented as mean ± SEM (n=5–9); Two-tailed, unpaired Student's *t*-test, * indicates P <0.05. **(e)** Representative magnetic resonance images (MRI) at the level of the papillary muscle at diastole and systole confirms left ventricular chamber dilation and systolic dysfunction in G2 mice. Scale bar 5 mm. Source data are shown in Supplementary Table S1.

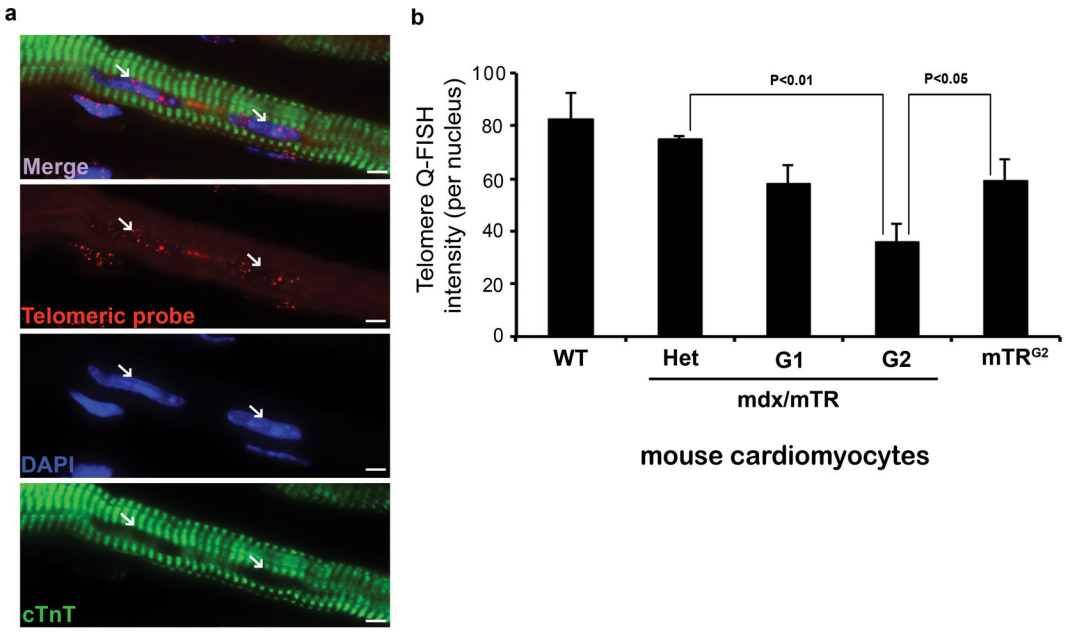

Figure 3. Telomere Q-FISH analysis of cardiac sections from mice

(a) Representative Telomere Q-FISH images (red telomeric probe; blue DAPI-stained nuclei, and green immunofluorescence of cardiac Troponin T reveals striated cardiomyocytes). White arrows indicate nuclei within cardiomyocytes. Scale bar 400 μm.

(b) Quantification of telomere shortening in cardiomyocytes represents the intensity sum of all telomere pixels ($Cy3^+$ telomeres) divided by the intensity sum of all nuclear DNA pixels of the entire nucleus (DAPI). A total of 3 hearts per genotype were analyzed. The number of nuclei scored: WT (N=394), HET (N=303), G1 (N=355), G2 (N=414), mTR^{G2} (N=390). Data are represented as mean ± SEM; Two-tailed, unpaired Student's *t*-test, P values are indicated. Source data are shown in Supplementary Table S1.

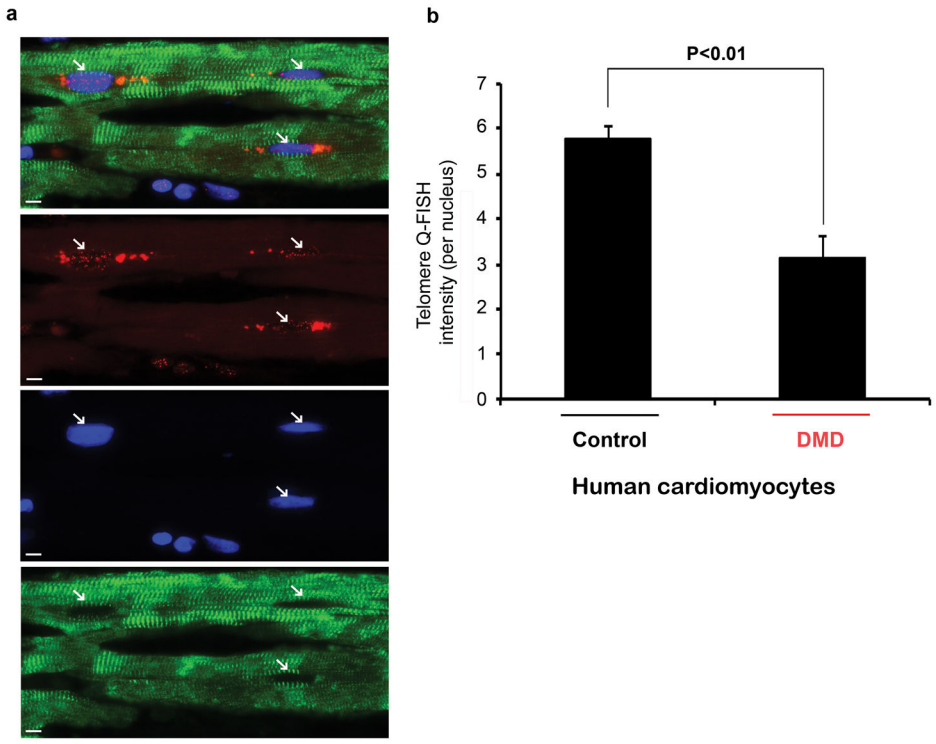

Figure 4. Telomere Q-FISH analysis of cardiac section from human DMD hearts

(a) Representative Telomere Q-FISH images (red, telomeric probe; blue, DAPI-stained nuclei and green, cardiac Troponin T staining). Scale bar 400 μm. **(b)** Quantification of telomere shortening in cardiomyocytes represents the intensity sum of all telomere pixels ($Cy3^+$ telomeres) divided by the intensity sum of all nuclear DNA pixels of the entire nucleus (DAPI). A total of 3 control and 4 DMD cardiac samples were analyzed and the number of nuclei scored: Control 1 (N=70), Control 2 (N=69), Control 3 (N=65), DMD 1 (N=42), DMD 2 (N=94), DMD 3 (N=65) and DMD 4 (N=72). Data are represented as mean ± SEM; Two-tailed, unpaired Student's *t*-test, P value is indicated. Source data are shown in Supplementary Table S1.

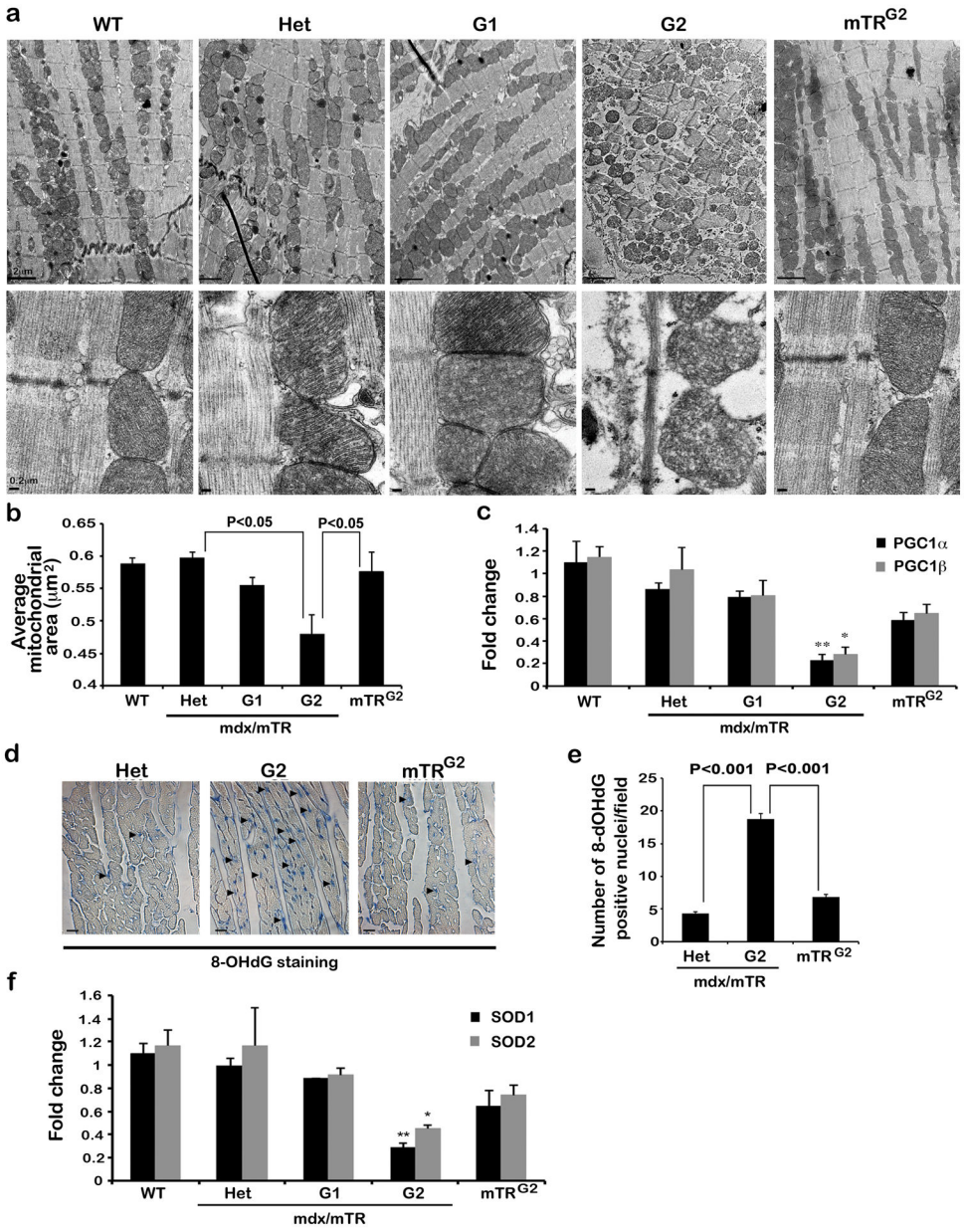

Figure 5. Telomere dysfunction is associated with mitochondrial abnormalities and oxidative stress

(a) Representative longitudinal sections of murine cardiac muscle by transmission electron micrographs show cellular edema, loss of thick and thin filaments and mitochondrial fragmentation in G2 hearts compared to control images. Scale bar 2μm. Lower panel shows a closer look of mitochondria. Note the loss of cristae of G2 hearts. Scale bar 0.2 μm. **(b)** Quantification of mitochondrial area (n=3 animals per genotype, 3 different areas of the left ventricle per heart, and n=10 photos per area analyzed); Two-tailed, unpaired Student's *t*-test, P values are indicated. **(c)** Q-RT-PCR analysis for PGC1α and PGC1β gene expression show decreased levels in the G2 hearts. (n=3 hearts per genotype; data are represented as mean ± SEM; Two-tailed, unpaired Student's *t*-test, * indicates P<0.05 and ** P<0.01). **(d)**

Immunohistochemistry reveals increased number of 8-OHdG-positive nuclei in the hearts of 32-week old G2 animals. Scale bar 400 μm. **(e)** Quantification of the 8-OHdG staining. Data are represented as mean ± SEM. (n=3 hearts per genotype; >10 images per heart were analyzed), Two-tailed, unpaired Student's *t*-test, P values are indicated. **(f)** Q-RT-PCR analyses of levels of anti-oxidative enzymes (SOD1 and SOD2) show decreased levels in the hearts of G2 mice. (n=3 hearts per genotype; data are represented as mean ± SEM); Two-tailed, unpaired Student's *t*-test, * indicates $P<0.05$ and ** $P<0.01$. Source data are shown in Supplementary Table S1.

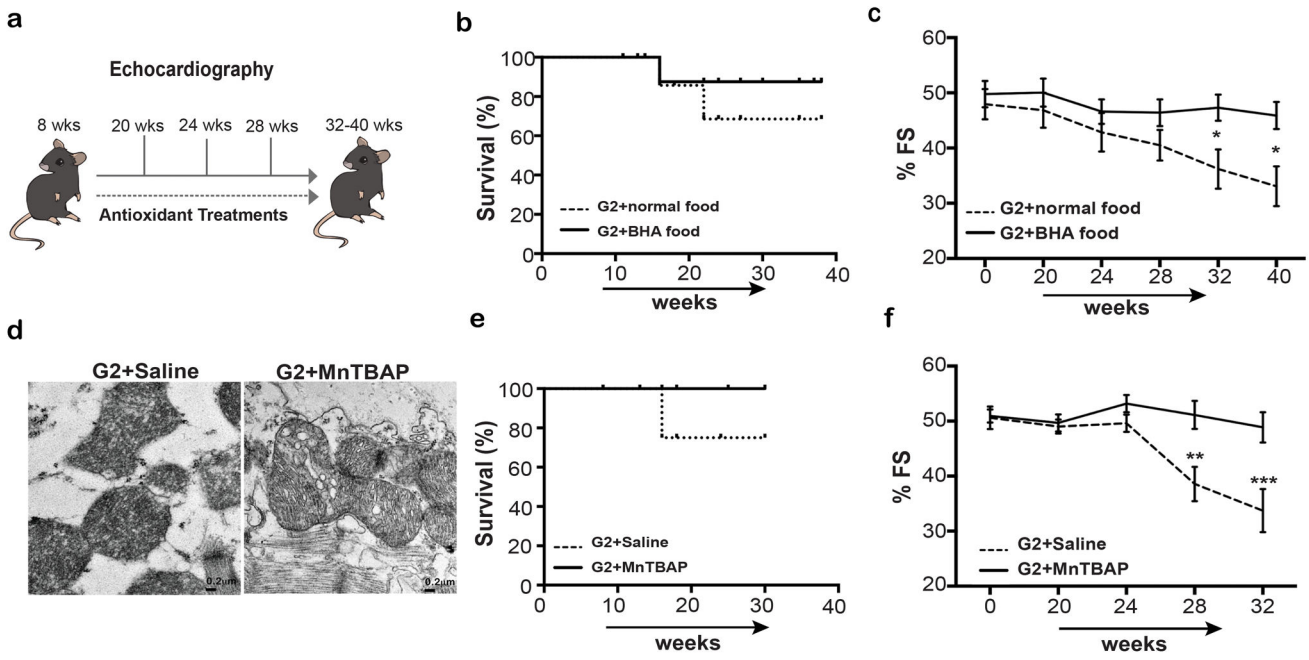

Figure 6. Antioxidant treatment increased survival and improved cardiac function

(a) Scheme of experimental procedure. Mice were treated with anti-oxidant (BHA food or MnTBAP injection) at 8 weeks old and tested monthly for cardiac function by echocardiography until 32–40 weeks old. **(b)** Decreased mortality of G2 mice treated with BHA food. Animals tested: G2-BHA food (n=10), G2-Normal food (n=10). **(c)** Echocardiography measurements (by means of fractional shortening as %FS) showed comparable increase in cardiac function of G2 mice treated with BHA food compared to controls. ANOVA followed by Bonferoni test for multiple comparisons; * indicates $P<0.05$. **(d)** Representative longitudinal sections of murine cardiac muscle of MnTBAP-injected G2 hearts show improved mitochondria morphology. Note that some formation of cristae is evident in G2 MnTBAP-injected cardiac mitochondria. Scale bar 0.2 μm **(e)** Extension of survival in G2 mice treated with daily injections of MnTBAP. Animals tested: G2-MnTBAP (n=10), G2-Saline (n=10). **(f)** Improved cardiac function in MnTBAP-injected compared to saline-injected G2 hearts. ANOVA followed by Bonferoni test for multiple comparisons; ** indicates $P<0.01$ and *** $P<0.001$. Source data are shown in Supplementary Table S1.